Optimal Excitatory and Inhibitory Balance for High Learning Performance in Spiking Neural Networks with Long-Tailed Synaptic Weight Distributions

Ibuki Matsumoto
Graduate School of Information and Computer Science
Chiba Institute of Technology
Chiba, Japan
ORCID: 0000-0002-3501-5304

Sou Nobukawa
Graduate School of Information and Computer Science
Chiba Institute of Technology
Chiba, Japan
ORCID: 0000-0001-7003-6912

Tomoki Kurikawa
Department of Complex and Intelligent Systems
Future University Hakodate
Hokkaido, Japan
ORCID: 0000-0003-1475-2812

Nobuhiko Wagatsuma
Department of Information Science
Toho University
Chiba, Japan
ORCID: 0000-0001-9090-9223

Yusuke Sakemi
Research Center for Mathematical Engineering
Chiba Institute of Technology
Chiba, Japan
ORCID: 0000-0002-0274-9491

Takashi Kanamaru
School of Advanced Engineering
Kogakuin University
Tokyo, Japan
ORCID: 0000-0001-5018-0570

Nina Sviridova
Department of Intelligent Systems
Tokyo City University
Tokyo, Japan
ORCID: 0000-0001-5850-0604

Kazuyuki Aihara
International Research Center for Neurointelligence
The University of Tokyo
Tokyo, Japan
ORCID: 0000-0002-4602-9816

2023 International Joint Conference on Neural Networks (IJCNN) | 978-1-6654-8867-9/23/$31.00 ©2023 IEEE | DOI: 10.1109/IJCNN54540.2023.10191709

***Abstract*—Excitatory/inhibitory (E/I) balance is significantly associated with cognitive function. Its imbalance impairs cognitive function, particularly in patients with psychiatric disorders. Recent physiological and modeling findings show that excitatory postsynaptic potentials (EPSPs) have a long-tailed distribution and contribute to the generation of spontaneous activity. Moreover, this spontaneous activity and its response to the external stimulus significantly alternate under the different E/I balance. However, the effects of the E/I balance under long-tailed EPSPs at the functional level remain unknown. Hence, to elucidate this relationship, we constructed a reservoir computing (RC) model generating the long-tailed distribution of EPSPs and investigated the effect of the E/I balance on the learning performance of RC in the memory capacity (MC) task, which measures how correctly delayed input signals can be reproduced. The results revealed that an appropriate E/I balance maximized the MC. This high MC was realized by recurrent spike propagation under long-tailed EPSPs. These findings contribute to the understanding of the effect of the E/I balance in physiologically relevant neural networks.**

***Index Terms*—E/I balance, long-tailed distribution of EPSPs, reservoir computing, memory capacity**

I. Introduction

Cognitive functions such as learning, memory, and perception, are produced by multiple hierarchical interactions of neural activities among different brain regions [1]. A neural network composed of excitatory and inhibitory neurons (e.g., neurons with two main neurotransmitters, i.e., glutamatergic [excitatory] and GABAergic [inhibitory] synaptic connections) is the most representative interaction of neural activity at the microcircuit level [2]. The balance of excitatory and inhibitory (E/I balance) plays an essential role in coordinating cognitive functions through gamma-band activity (30–80 Hz) [3]. Therefore, the E/I imbalance can be an underlying cause of psychiatric disorders with their associated cognitive deficits [3]–[6], such as schizophrenia (SCZ) and autism spectrum disorder (ASD) [2], [7], [8]. Clinically, the influence of E/I imbalance can be detected using neuroimaging techniques such as proton magnetic resonance spectroscopy (^{1}H-MRS), electroencephalography (EEG), magnetoencephalography (MEG), and functional magnetic resonance imaging (fMRI) [1], [2], [9]. Neuroimaging with ^{1}H-MRS has revealed hyper-excitatory synaptic connections in the SCZ neural network [2]. Using

neuroimaging with EEG and MEG, a large number of studies utilizing their high temporal resolution have demonstrated the alternations in gamma-band activity caused by E/I imbalance due to psychiatric pathologies [3]–[5].

Such neuroimaging approaches capture the macroscopic alternations of neural activity emerging from neural interactions at large neural population levels [1], [2], [9]. However, this approach cannot reveal an explicit link between microcircuit-level impairment of neural networks typified as local E/I imbalance and dynamic alternation of neural activity [10]. To address these difficulties, a computational approach is an effective solution, because it can reveal the causes of the alternations in neural activity through the reproduced neural activity in the model-embedded microcircuit structures involving local E/I imbalance [2], [11]–[14]. In particular, this approach revealed that the E/I balance coordinates the level of randomness and regularity of spiking patterns; consequently, the optimized spiking patterns achieve sophisticated information propagation [11], [12]. Shashaank $et\ al.$ and John $et\ al.$ demonstrated that the impairment of the local E/I balance leads to pathological neural network activity and subsequent perceptual dysfunction, which are often related to ASD [11] and SCZ [12].

Over the past decade, notable properties of such E/I-balanced neural networks, particularly the characteristics of microcircuits in the cerebral cortex, have been revealed [13], [14]. Specifically, the excitatory postsynaptic potential (EPSP), which is the elevated potential of a neuron when it receives a signal via an excitatory synapse, forms a long-tailed distribution with respect to the strength of the connection between excitatory neurons [15]. In this distribution, sparse-strong (long-tailed part of the distribution) and dense-weak (mode part of the distribution) synaptic weights, which play signal and noise roles, respectively, are observed in synaptic connectivity [16]. These components in this long-tailed EPSPs distribution contribute to enhancing the signal propagation through the mechanism of stochastic resonance [16]–[19]. Moreover, Nobukawa $et\ al.$ showed that long-tailed EPSPs distribution significantly enhances the E/I ratio dependency of the response characteristics against perceptual signals compared with the conventionally assumed non-long-tailed EPSP distribution [13]. Therefore, subsequent investigations on the E/I balance in networks with long-tailed EPSPs at the functional level are required.

Reservoir computing (RC) [20]–[22] is a valid approach for evaluating the functionality of networks with long-tailed EPSPs under different conditions using an E/I balance. RC is a computational framework based on a recurrent neural network (RNN), and the input data are transformed into spatiotemporal patterns in the reservoir (as shown in Fig. 1) [20]–[22]. In contrast to other RNNs, the connection weights are trained only by the readout weights ($\mathrm{W_{out}}$). Additionally, RC can investigate the functionalities of brain connectivity by incorporating network characteristics into a reservoir [23]–[25]. In particular, Matsumoto $et\ al.$ evaluated the functionality of a long-tailed EPSPs distribution by embedding this distribution in the reservoir of the RC [26]. The results showed that a long-tailed EPSPs distribution enhanced the RC performance through gamma-band dynamic neural activity. Specifically, the memory capacity and accuracy of nonlinear time-series prediction were enhanced by gamma-band activity in a network with strong EPSPs.

In this context, we hypothesized that evaluating the functionality of the E/I balance under a long-tailed EPSPs distribution using RC might reveal the novel functional side of the activity produced from excitatory and inhibitory neural interactions in physiologically relevant neural networks. To verify this hypothesis, we investigated the computational capability of reservoir computing depending on the E/I balance using the memory capacity task, which is a representative evaluation method for reservoir computing.

II. Related Works

A. Modeling for spontaneous activity

Teramae et al. showed that the long-tailed distribution of EPSPs evokes spontaneous activity in the spiking neural network model [16]. They exhibited that the mechanism of stochastic resonance induced by the long-tailed distribution of EPSPs contributes to spontaneous firing activity which maintains the continuously and irregularly spiking activity. Specifically, the distributions of weak-dense synaptic weights and strong-sparse synaptic weights play a role in noise and signal in the phenomenon of stochastic resonance, respectively. Spontaneous activity is one of the essential factors for learning and memory [27], [28]; therefore, the consideration of the long-tailed EPSPs contributes to the understanding of the cognitive dynamics of the brain.

B. RC model

RC model is one of the RNNs [20]–[22], and RC is utilized not only to improve the computational performance, but also to elucidate the brain's mechanisms [23], [29]. For example, the connections of topology and weight distribution in the neural circuit have been examined [23], [30]. In particular, a RC model with long-tailed EPSPs showed they contributed to a high memory capacity and prediction accuracy [31]. This indicated that a few strong connections in the long-tailed part are important for information propagation in the recurrent connection. However, the previous study only focused on the importance of the long-tailed distribution [31]. Thus, further studies utilizing such a model are needed to reveal other physiological characteristics.

C. Computational approaches to the understanding of E/I balance with long-tailed EPSPs

The balance of E/I is optimized at the microcircuit level, such as in the ratio of glutamate/GABA or the number of synapses of excitatory/inhibitory neurons [32]. It is well known that an imbalance of excitability and inhibition is related to psychiatric disorders such as ASD and SCZ [11], [12]. In a clinical pathology experiment, animals were administered drugs to reveal the influence of the E/I balance on cognitive

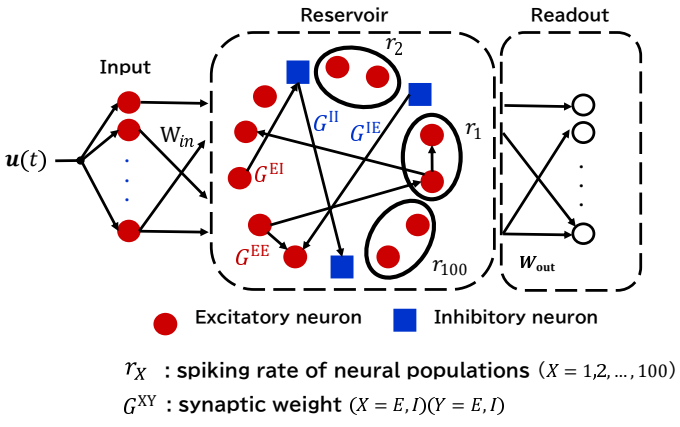

Fig. 1. Schematic of reservoir computing (RC) model with long-tailed distribution of excitatory postsynaptic potentials (EPSPs). Reservoir is composed of a spiking neural network (SNN) with long-tailed EPSP distribution produced by Teramae *et al.* [16].

functions [33], [34]. On the other hand, computational modeling is useful for manipulating excitability and inhibition at the microcircuit level. It is worth revealing the contribution of local circuit characteristics such as E/I balance and long-tailed EPSPs on brain functions. Thus, the functionality of E/I balance in SNN with long-tailed EPSPs should be evaluated.

III. Methods

A. Reservoir computing (RC) model

1) Neural network for reservoir computing: We constructed an RC model that includes an SNN with a long-tailed distribution of EPSPs based on the model by Teramae *et al.* [16]. An overview of the proposed model is shown in Fig. 1. All the neurons behaved accordingly with the leaky integrate-and-fire model. The RC model consists of an input, reservoir, and readout. The input layer consists of 20 excitatory neurons ($N_{\rm in} = 20$), and the reservoir consists of 10,000 excitatory ($N_{\rm E} = 10,000$) and 2,000 inhibitory ($N_{\rm I} = 2,000$) neurons. In this study, the spiking rates of the excitatory neural populations in the reservoir were used to train in the readout. In this study, the ridge regression was used as the learning algorithm. 10,000 excitatory neurons in the reservoir were classified into 100 excitatory neural populations to obtain a continuous firing rate. In the readout, the synaptic weight ($\rm W_{out}$) from the neural populations in the reservoir to the output of the RC was trained using ridge regression.

The input neurons propagate an external input/stimulus $u(t)$ to the reservoir neurons as spikes. The membrane potential of the input neuron $v_i(t)(i = 1, 2, ..., 20)$ is defined as follows:

$$\frac{dv_i}{dt} = -\frac{1}{\tau_{\rm in}}(v_i - V_{\rm L}) + u(t), \tag{1}$$

$$\text{if } v_i(t) \geq V_{\rm thr}\ [\rm mV],\ \text{then } v_i(t) \to V_{\rm r}\ [\rm mV], \tag{2}$$

where $\tau_{\rm in}$, $V_{\rm L}$, and $u(t)$ denote the decay constant of the membrane ($\tau_{\rm in} = 20$ [ms]), the reversal potential of leak ($V_{\rm L} = -70$ [mV]), and the external input changes every 1 [ms], respectively. The input neurons spiked when the membrane potential exceeded the threshold value ($V_{\rm thr} = -50$ [mV]). After spiking, the membrane potentials were reset ($V_{\rm r} = -60$ [mV]).

The membrane potential of the reservoir neuron $v_j(t)$ that receives spikes from the input neurons is defined by

$$\frac{dv_j}{dt} = -\frac{1}{\tau_m}(v_j - V_{\rm L}) - g_{\rm EY,j}(v_j - V_{\rm E}) - g_{\rm IY,j}(v_j - V_{\rm I}) + \sum_i W^{\rm in}_{j,i} \sum_{S_i} \delta(t - s_i), \quad {\rm Y} = {\rm E}, {\rm I}. \tag{3}$$

The reservoir neurons consist of excitatory ($j = 1, 2, \cdots, N_{\rm E}$) and inhibitory ($j = N_{\rm E} + 1, \cdots, N_{\rm E} + N_{\rm I}$) neurons. The decay constants of the membrane τ_m were 20 [ms] (excitatory neurons) and 10 [ms] (inhibitory neurons). The reversal potentials of synaptic currents for excitatory/inhibitory neurons and for leak current were $V_{\rm E} = 0$ [mV], $V_{\rm I} = -80$ [mV], and $V_{\rm L} = -70$ [mV], respectively. In addition, the connectivity between the input and reservoir neurons was random, and the coupling probability was 0.1. $\delta(t)$ is a delta function. Therefore, when the i-th input neuron is fired at time $t = s_i$, the membrane potentials of the reservoir neurons receive the spikes from the input neurons with an increase in voltage $W^{\rm in}$ [mV]. In this study, we set $W^{\rm in}$ = 1.0 [mV]. Reservoir neurons also fired when the membrane potentials reached the threshold potential $V_{\rm thr} = -50$ [mV]. Subsequently, the potentials were reset to $V_{\rm r} = -60$ [mV], as well as the input neurons by Eq. (2). According to Eq. (3), the excitatory and inhibitory neurons in SNN transmitted the information with each other by using their conductance $g_{{\rm EY},j}(t)$ [$\rm ms^{-1}$] (excitatory) and $g_{{\rm IY},j}(t)$ [$\rm ms^{-1}$] (inhibitory). Y denotes the synaptic destination of neurons (excitatory neurons (E) or inhibitory neurons (I)). Conductance is defined as follows:

$$\frac{dg_{{\rm XY},j}}{dt} = -\frac{g_{{\rm XY},j}}{\tau_s} + \sum_k G^{\rm XY}_k \sum_{s_k} \delta(t - s_k - d_k), \quad {\rm X} = {\rm E}, {\rm I}, {\rm Y} = {\rm E}, {\rm I}, \tag{4}$$

where τ_s, s_k, and d_k denote the decay constant of the membrane ($\tau_s = 2$ [ms]), the spiking time of the input from k-th neuron, and the synaptic delay, respectively. $G^{\rm IE}_k$, $G^{\rm II}_k$, $G^{\rm EI}_k$, and $G^{\rm EE}_k$ represent the synaptic weights of inhibitory-to-excitatory, inhibitory-to-inhibitory, excitatory-to-inhibitory, and excitatory-to-excitatory neurons, respectively. When the k-th presynaptic neuron fires at time $t = (s_k + d_k)$, the spike weighted by $G^{\rm XY}_k$ is transmitted to the j-th postsynaptic neuron.

The distribution of EPSPs can be approximated as lognormal distribution, as defined by

$$p(x) = \frac{\exp[-(\log x - \mu)^2/2\sigma^2]}{\sqrt{2\pi}\sigma x}, \tag{5}$$

where x is the amplitude of the EPSPs (see Fig. 2) [16], [35], [36]. We set the values as $\sigma = 1.0$ and $\mu - \sigma^2 = \log(0.2)$ in this approximation. We calculated the values of

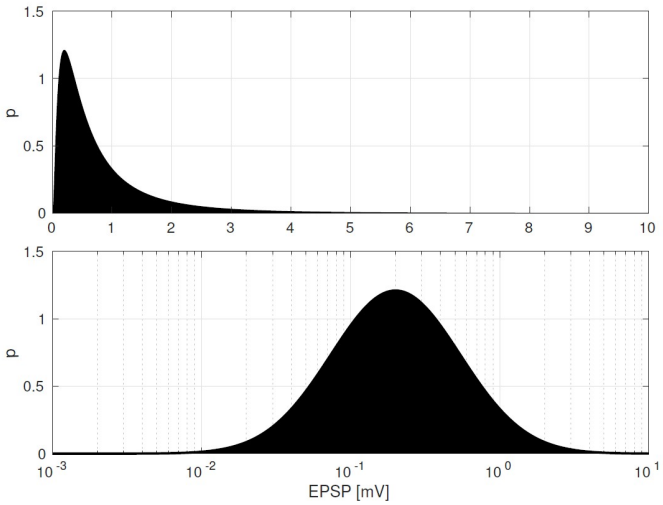

Fig. 2. Schematic of the long-tailed distribution of excitatory postsynaptic potentials (EPSPs) calculated by Eq. (5). Top: the shape of the long-tailed distribution of EPSPs. Bottom: the distribution with logarithmic scale to EPSPs. This distribution describes many weak (EPSP $<$ 2 [mV]) and sparse-strong (EPSP $\geq$ 2 [mV]) synaptic potentials. In this study, to the right of this distribution (EPSP $\geq$ 2 [mV]) is regarded as a long tail. It is known that this distribution has an essential role in the neural network of the brain.

the EPSPs using Eq. (5) to be biologically plausible. Here, if the calculated value of the EPSPs exceeds 20 [mV], the value is regenerated to be within the range of 20 [mV] from Eq. (5). In addition, the EPSP was an observable value; thus, we translated it into the synaptic weight G_k^{EE} based on a previous study [36], which considered the relationship between the EPSP and G_k^{EE} : $G_k^{\mathrm{EE}} = V_{\mathrm{EPSP}}/100$.

2) Parameter settings for the synaptic weights between excitatory and inhibitory neurons: Regarding the parameter settings of the neurons and their connectivity in the SNN, in this study, most parameters involving log-normal EPSP distributions followed those used by Teramae $etal.$ [16]. However, to examine the effect of the E/I balance on the learning performance of the RC, we changed the synaptic weights of the excitatory and inhibitory neurons from the original parameters. For the parameters used by Teramae $et\ al.$ [16], the synaptic weights were set to $G_j^{\mathrm{EI}} = 0.018$ (excitatory-to-inhibitory), $G_j^{\mathrm{IE}} = 0.002$ (inhibitory-to-excitatory), and $G_j^{\mathrm{II}} = 0.0025$ (inhibitory-to-inhibitory). Under this condition, the SNN exhibits spontaneous firing activity [16], [35]. Further, we varied the synaptic weights (G_j^{EI} and G_j^{IE}) to investigate the effects of the synaptic weights of excitatory-to-inhibitory and inhibitory-to-excitatory neurons. Specifically, when the synaptic weights were $G_j^{\mathrm{IE}} = 0.002$ (the original value) [16], we changed $G_j^{\mathrm{EI}} = 0.014, 0.018, 0.04, 0.05, 0.07, 0.10$ and 0.15.

With respect to the other parameters, the connection probabilities and values of the synaptic delays were set as fixed values based on previous studies [16], [35]. The connection probabilities were set to 0.1 (excitatory-to-inhibitory) and 0.5 (except for the connection between excitatory neurons). In addition, we randomly set the value of the synaptic delays within the range of 1-3 [ms] (excitatory-to-excitatory) and 0-2 [ms] (others). We adjusted for the probability of failure for the transmission between excitatory neurons as follows: $p_{\mathrm{E}} = a/(a + \mathrm{EPSP})$, where $a = 0.1$ [mV] [15], [16]. The parameters for our model are listed in Table I.

3) Learning method: Numerical simulations were performed for 50 [s]. During the simulations, we recorded the spiking rate of each excitatory neural population that was classified in advance. The spiking activities of neural populations were averaged in 0.1 [ms] in the simulations. Specifically, to calculate the spiking rate of the X-th neural population r_{X} [Hz] (neural population number: $\mathrm{X} = 1, 2, 3, ..., 100$), we averaged each neural population composed of 100 neurons per unit time as follows:

$$r_{\mathrm{X}}(t) = 10^3 \frac{S_{\mathrm{X}}(t)}{100\Delta t},\ \mathrm{X} = 1, 2, 3, ..., 100. \tag{6}$$

Here, S_{X} denotes the spike frequency, that is, the number of spikes of a time bin of 0.1 [ms] in the X-th neural populations. r_{X} [Hz] is smoothed using a window of 10 [ms] with a Gaussian filter.

In this study, the RC reproduced the desired signal by mapping the firing rate in the reservoir to a linear output. We utilized ridge regression as the linear regression algorithm to acquire the output of the RC as follows:

$$\mathbf{W}_{\mathrm{out}} = ((\mathbf{X}^{\mathsf{T}}\mathbf{X} + \alpha\mathbf{I})^{-1}\mathbf{X}^{\mathsf{T}}\mathbf{D})^{\mathsf{T}}. \tag{7}$$

where α and $\mathbf{I}$ denote the non-negative regularization factor and identity matrix, respectively. $\mathbf{X} = (r_X(1), ..., r_X(T))^{\mathsf{T}}$ is a matrix of the spiking rate for 100 neural populations ($T \times 100$). T indicates the duration of learning. $\mathbf{D} = (y_d(1), ..., y_d(T))^{\mathsf{T}}$ denotes the desired output matrix ($T \times 1$). Learning output weights $\mathbf{W}_{\mathrm{out}}$ correspond to solving a system of linear equations [20]. Therefore, the output of RC $\mathbf{y}(t)$ was calculated using the spiking rate of the neural populations converted to spatiotemporal patterns against the input as follows:

$$\mathbf{y}(t) = \mathbf{W}_{\mathrm{out}}\mathbf{X}. \tag{8}$$

In this study, we set $\alpha = 0.01$ because the MC was maximized. The simulation duration for each trial was 50 [s]. In this simulation, the first and last 500 [ms] had transient periods; therefore, we removed these periods. In other words, the learning duration is $T = 49,000$ [ms] (500 [ms] $\leq T \leq$ 49,500 [ms]).

B. Evaluation Index

1) Memory capacity task: We investigated memory capability to evaluate the learning performance of the RC. In the training section, the RC is trained to generate its output at the delayed point of the input. Memory capacity (MC) task [37] measures how correctly delayed input signals can be reproduced. In the MC task, an input series $\mathbf{u}(t)$ is a series of uniform, random number taken from [0, 0.01]. As stated before, the RC outputs the delayed point of the input; therefore, the desired series $y_d(t)$ is τ delayed the point of

TABLE I
PARAMETERS FOR OUR SPIKING NEURAL NETWORK

Parameters	Descriptions	Values	References for parameter values
τ_{in}	Decay constant of the membrane	20 [ms]	[16]
V_{L}	Reversal potential of leak	-70 [mV]	[16]
V_{thr}	Threshold potential	-50 [mV]	[16]
V_{r}	Reset potential	-60 [mV]	[16]
τ_{m}	Decay constant of the membrane for excitatory neuron	20 [ms]	[16]
	Decay constant of the membrane for inhibitory neuron	10 [ms]	[16]
V_{E}	Reversal potential of synaptic current for excitatory neuron	0 [mV]	[16]
V_{I}	Reversal potential of synaptic current for inhibitory neuron	-80 [mV]	[16]
W^{in}	Synaptic weight after spiking from input neuron	1.0 [mV]	[31]
τ_{s}	Decay constant of the membrane	2 [ms]	[16]
G^{EE}	Synaptic weight of excitatory-to-excitatory neurons	*	[16], [35]
G^{EI}	Synaptic weight of excitatory-to-inhibitory neurons	**	[16], [35]
G^{IE}	Synaptic weight of inhibitory-to-excitatory neurons	0.002	[16], [35]
G^{II}	Synaptic weight of inhibitory-to-inhibitory neurons	0.0025	[16], [35]

* G^{EE} follows the long-tailed distribution. ** G^{EI} is changed from 0.014 to 0.10 to adjust the balance of excitability/inhibition.

input, that is, $y_d(t) = u(t-\tau)$. The random numbers used as inputs were rescaled to a slower input time series. Originally, the sampling frequency was 1 [ms], we rescaled it to 100 [ms] to adjust the main frequency component of the SNN. The MC was defined by

$$\mathrm{MC}_\tau = \frac{\mathrm{cov}^2(\mathbf{u}_\tau, \mathbf{y})}{\sigma^2(\mathbf{u}_\tau)\sigma^2(\mathbf{y})}, \tag{9}$$

$$\mathrm{MC} = \sum_{\tau=1}^{\mathrm{T}} \mathrm{MC}_\tau, \tag{10}$$

where $\mathrm{cov}(\mathbf{u}_\tau, \mathbf{y})$ and σ^2 denote the covariance between the input $\mathbf{u}_\tau$ and the output series of the RC and the variance, respectively. In this study, we investigated the MC for 1 [ms] $\leq \tau \leq$ 1,000 [ms]. Because MC represents the correlation between the input and output of the RC, MC_τ exhibits values from 0 to 1. For example, when the MC is 1, this indicates the RC can accurately reproduce information from the previous τ step. We performed the simulation 10 times with different random seeds; that is, the random connections between neurons were different each time. The input signal was changed stochastically.

IV. RESULTS

1) Memory capacity depends on excitatory/inhibitory ratio: To investigate the role of E/I balance, we analyzed the effect of changing G^{EI} on MC. In high G^{EI}, inhibitory neurons are strongly excited by excitatory neurons, resulting in inhibitory-dominant neural activity. In contrast, in low G^{EI}, inhibitory neurons are strongly suppressed by excitatory neurons, resulting in excitatory-dominant neural activity. Figure 3 shows MC when the excitatory-to-inhibitory synaptic weights (G^{EI}) were varied ($0.014 \leq G^{\mathrm{EI}} \leq 0.15$) and when the value of inhibitory-to-excitatory synaptic weights (G^{IE}) was kept at 0.002. From these results, we observed an inverted-U-shaped MC profile (the peak of the MC located at $G^{\mathrm{EI}} = 0.04$). This result determined the optimal E/I balance.

These results beg the question of why the intermediate G^{EI} value demonstrates the highest performance in MC. To answer this question, we demonstrated the dynamics of the reservoir for different G^{EI}. Figure 4 shows the time series of the input signals and the typical spiking activity in all excitatory neural populations ($G^{\mathrm{EI}} = 0.014, 0.04, 0.15$). At $G^{\mathrm{EI}} = 0.014$ (in Fig. 4b), the large fluctuation due to hyper-excitatory activity; therefore, the spiking rate does not correspond to the input signal. On the other hand, in $G^{\mathrm{EI}} = 0.15$ (in Fig. 4d), the low spiking activity due to the inhibitory-dominant state cannot represent the response of the input signal. At $G^{\mathrm{EI}} = 0.04$ (in Fig. 4c), optimal levels of spiking activity with moderate fluctuations were evident, and a response against the input signal can be achieved. As a result, the spiking activity facilitates the MC task.

2) Recover the low memory capacity due to the E/I imbalance: We found that an intermediate G^{EI} value enabled the best performance in MC, whereas E/I imbalance reduced the performance. Consequently, it should be determined whether a change in G^{IE} can improve the E/I balance and MC performance. Figure 5 shows the compensation for low MC by increased synaptic inhibition G^{IE} under the condition of excitatory dominance owing to the lack of feedback inhibition of excitatory neurons in Fig. 3 (low MC ($\approx$116) at $G^{\mathrm{EI}} = 0.014$). Moderate inhibition of inhibitory-to-excitatory neurons rescued low MC and exhibited an inverted-U-shaped pattern. Thus, the performance degradation of RC due to the impairment of feedback inhibition was recovered by enhancement of inhibition.

V. DISCUSSION

In this study, to elucidate the relationship between the E/I balance under the physiologically observed conditions and

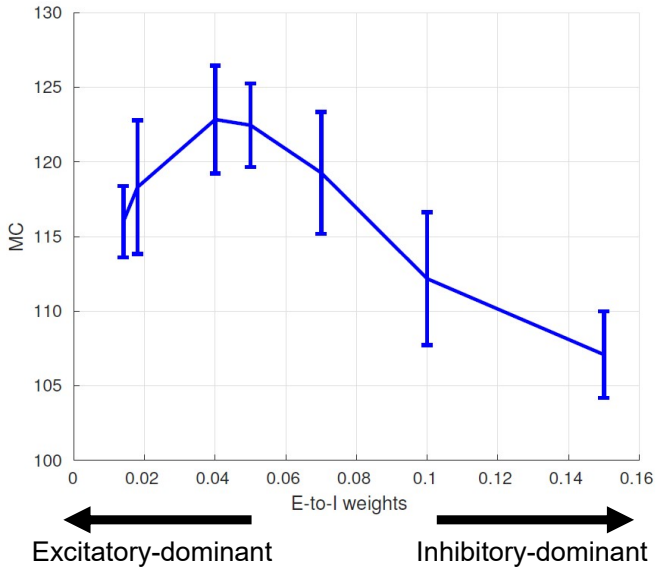

Fig. 3. Transition of memory capacity (MC) dependence on excitatory-to-inhibitory synaptic weights G^{EI} in the cases of $G^{\mathrm{IE}} = 0.002$. The blue curve and error bars indicate the results of averaged MCs and standard deviation over 10 trials, respectively. The MC exhibited an inverted U-shaped, i.e., the appropriate synaptic weights of excitatory-to-inhibitory at $G^{\mathrm{EI}} = 0.04$ were observed to maximize the MC. The decreased synaptic weights of excitatory-to-inhibitory weaken the feedback inhibition from inhibitory neurons, which results in hyperexcitation of excitatory neurons (i.e., excitatory dominance). On the other hand, the increased feedback inhibition suppresses the activity of excitatory neurons (i.e., inhibitory dominance). These states exhibited the low MC.

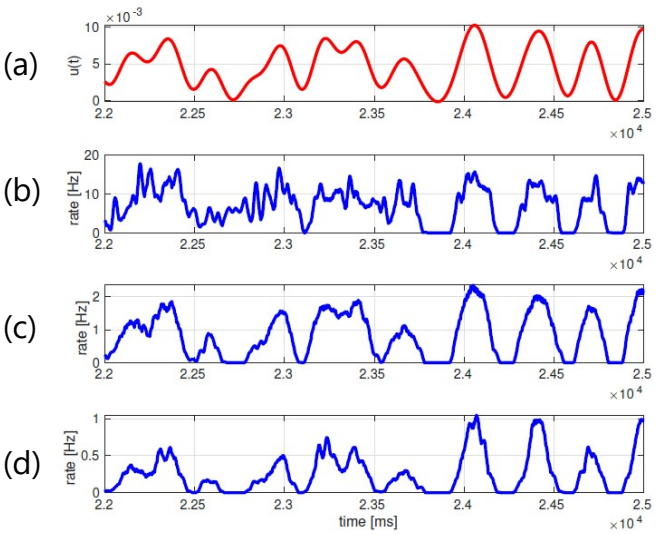

Fig. 4. Spiking activity of all excitatory neural populations in SNN in Fig. 3. 4a Input signal to RC. 4b Spiking rate under the excitatory dominance ($G^{\mathrm{EI}} = 0.014$; MC $\approx$ 116). 4c Spiking rate under the optimal E/I balance ($G^{\mathrm{EI}} = 0.04$; MC $\approx$ 122). 4d Spiking rate under the inhibitory dominance ($G^{\mathrm{EI}} = 0.15$; MC $\approx$ 107).

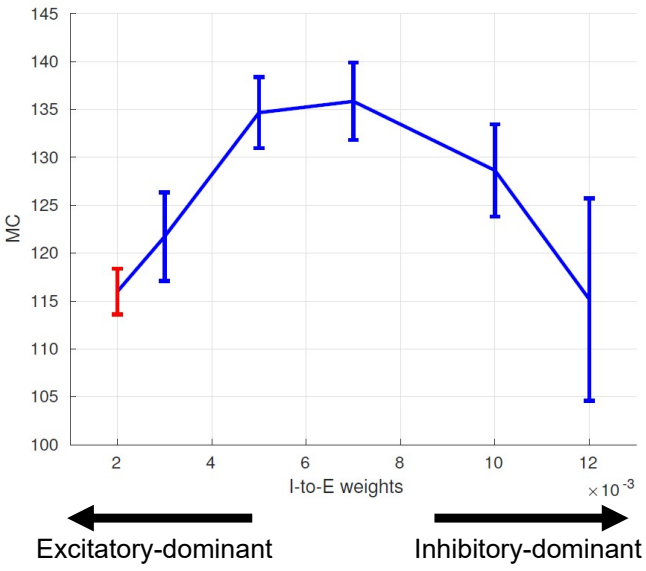

Fig. 5. MC dependence on the synaptic weights of inhibitory-to-excitatory neurons G^{IE} as compensation of E/I imbalance. The red point and error bar correspond to the case of low MC ($G^{\mathrm{EI}} = 0.014$ (excitatory dominant state)) in Fig. 3. This state was recovered by adjusting the synaptic weights of inhibitory-to-excitatory neurons G^{IE}.

long-tailed distribution of EPSPs, the effect of E/I balance in the SNN embedded within EPSPs distribution on the typical performance of RC was explored. The dependence of performance on E/I balance was evaluated by changing synaptic weights between excitatory-to-inhibitory neurons. Our results showed that the performance of RC exhibited an inverted U-shape with changes in the synaptic weights.

First, we discuss the reasons why the MC dependence on the ratio of excitatory and inhibitory synaptic weights exhibited an inverted U-shape. In terms of the large excitatory-to-inhibitory synaptic weighting, $G^{\mathrm{EI}} > 0.04$ as shown in Fig. 3, increasing G^{EI} (i.e., approaching inhibitory dominance through feedback inhibition from activated inhibitory neurons to excitatory neurons, $G^{\mathrm{EI}} > 0.04$) led to a low MC. Under this condition for inhibitory dominance, the activity of the excitatory neurons was suppressed, and they exhibited low firing rates with low baseline activity of excitatory neurons (see $G^{\mathrm{EI}} = 0.15$ in Fig. 4d). Consequently, this silent neural activity cannot maintain past applied information (i.e., low MC). Conversely, decreasing the synaptic weights of excitatory-to-inhibitory neurons $G^{\mathrm{EI}} < 0.04$ also led to low MC owing to excitatory dominance. This is known as disinhibition, where defects in feedback inhibition led to the hyperexcitability of excitatory neurons. Hyperexcitability causes hypersensitivity to spike stimuli from the majority of weak synapses, such as noise, which leads to large internal fluctuations [13]. This large fluctuation can lead to inflexibility to the input [13] (see Fig. 4b); consequently, a detailed representation of the input signal fails. Impairments due to this deficit in feedback inhibition have been observed in several psychiatric disorders, such as epilepsy and SCZ [33], with associated impairments in cognitive function. Therefore, the degradation of MC observed in our results may correspond to these pathological conditions

[33], [38]. In contrast to the hyperexcitable and silent states, in the appropriate feedback inhibition ($G^{\mathrm{EI}} \approx 0.04$), the optimal internal deterministic fluctuations, which consist of recurrent spike propagation [16] from long-tailed EPSPs, contribute to enhancing learning performance of RC [31] (see "Appendix").

Second, the impact of restoring E/I balance was investigated; that is, the potential of improving disinhibition with MC impairment by increased inhibitory-to-excitatory synaptic weights (see Fig. 5). In the cortical working memory model, enhancing the inhibitory conductance (G^{IE}) improves disinhibition [12], [39]. Consequently, GABA compensation restores the E/I balance. Parallels are seen in pharmacology, where the use of drugs such as benzodiazepines, improves working memory deficits through disinhibition [40]. Therefore, the moderate enhancement of the effect of GABA release recovered the dysfunction of MC in our results, which is consistent with previous findings in both modeling and physiological studies.

Finally, the limitations of this study should be considered. It is well known that gamma oscillations are deeply associated with the fluctuation induced by the interactions among excitatory and inhibitory neurons [41]. Moreover, working memory impairment owing to abnormalities in gamma oscillations in SCZ can be observed with a reduced response in the gamma band [42]. This alternation of gamma oscillations must be evaluated by dynamic analysis to further reveal the effect of the E/I balance in networks with long-tailed EPSPs.

VI. Conclusion

This study revealed that an optimal E/I balance enhances the memory performance of SNN with long-tailed EPSPs in the RC model. The transition of MC exhibited an inverted U-shape for the modulation of the synaptic weights of excitatory-to-inhibitory and inhibitory-to-excitatory neurons. This high MC was realized by recurrent spike propagation under optimal internal fluctuations from long-tailed EPSPs. These findings contribute to the understanding of E/I balance in physiologically relevant neural networks.

Acknowledgments

This work was supported by JSPS KAKENHI for a Grant-in-Aid for Scientific Research (C) (Grant Number JP22K12183 (SN) and Grant Number JP20K07716 (TK (Tomoki Kurikawa))) and a Grant-in-Aid for Transformative Research Areas (A) JP20H05921 (SN, TK (Takashi Kanamaru), NS, and KA)), JST Moonshot R&D (Grant Number JPMJMS2021) (KA), AMED (Grant number JP23dm0307009) (KA), Institute of AI and Beyond of the University of Tokyo (KA).

Appendix

To investigate the contribution of long-tailed EPSPs to MC, cases with and without strong EPSPs were compared ($\geq$ 2 [mV]). Specifically, MC was investigated against the synaptic connection between excitatory neurons in the SNN with and without strong weights. The parameters (except for strong EPSPs) were the same as those in Fig. 3; the strong connections (EPSPs $\geq$ 2 [mV]) were removed. The results are shown in Fig. 6; compared to the strong ESPSs shown in Fig. 3, the MC significantly decreased and lost an inverted U-shape. It can be interpreted that the lack of excitatory and inhibitory dynamical interactions by strong EPSPs [26] caused these tendencies.

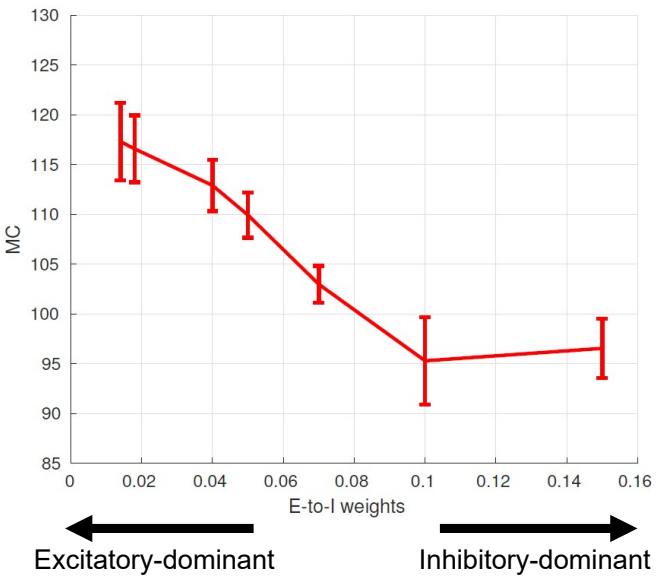

Fig. 6. Transition of memory capacity (MC) dependence on excitatory-to-inhibitory synaptic weights G^{EI} in the case of $G^{\mathrm{IE}} = 0.002$ in the case without strong EPSPs (EPSPs $\geq$ 2 [mV]). The red curve and error bars indicate the results of averaged MCs and standard deviation over 10 trials, respectively. The MC monotonically decreased toward increasing the synaptic weights of excitatory-to-inhibitory neurons (i.e., inhibitory dominance). Under the condition without strong EPSPs, an inverted U-shape was not observed in the transition of MC.

References

[1] O. Sporns, *Networks of the Brain*. MIT press, 2016.

[2] J. H. Foss-Feig, B. D. Adkinson, J. L. Ji, G. Yang, V. H. Srihari, J. C. McPartland, J. H. Krystal, J. D. Murray, and A. Anticevic, "Searching for cross-diagnostic convergence: neural mechanisms governing excitation and inhibition balance in schizophrenia and autism spectrum disorders," *Biological psychiatry*, vol. 81, no. 10, pp. 848–861, 2017.

[3] C. A. Bosman, C. S. Lansink, and C. M. Pennartz, "Functions of gamma-band synchronization in cognition: From single circuits to functional diversity across cortical and subcortical systems," *European Journal of Neuroscience*, vol. 39, no. 11, pp. 1982–1999, 2014.

[4] M. Bartos, I. Vida, and P. Jonas, "Synaptic mechanisms of synchronized gamma oscillations in inhibitory interneuron networks," *Nature reviews neuroscience*, vol. 8, no. 1, pp. 45–56, 2007.

[5] J. Lisman, "Excitation, inhibition, local oscillations, or large-scale loops: what causes the symptoms of schizophrenia?" *Current opinion in neurobiology*, vol. 22, no. 3, pp. 537–544, 2012.

[6] O. Yizhar, L. E. Fenno, M. Prigge, F. Schneider, T. J. Davidson, D. J. O ' shea, V. S. Sohal, I. Goshen, J. Finkelstein, J. T. Paz *et al.*, "Neocortical excitation/inhibition balance in information processing and social dysfunction," *Nature*, vol. 477, no. 7363, pp. 171–178, 2011.

[7] P. J. Uhlhaas and W. Singer, "High-frequency oscillations and the neurobiology of schizophrenia," *Dialogues in clinical neuroscience*, 2022.

[8] J. Rubenstein and M. M. Merzenich, "Model of autism: increased ratio of excitation/inhibition in key neural systems," *Genes, Brain and Behavior*, vol. 2, no. 5, pp. 255–267, 2003.

[9] K. J. Friston, "Modalities, modes, and models in functional neuroimaging," *Science*, vol. 326, no. 5951, pp. 399–403, 2009.

[10] P. Ritter, M. Schirner, A. R. McIntosh, and V. K. Jirsa, "The virtual brain integrates computational modeling and multimodal neuroimaging," *Brain connectivity*, vol. 3, no. 2, pp. 121–145, 2013.

[11] S. Vattikuti and C. C. Chow, "A computational model for cerebral cortical dysfunction in autism spectrum disorders," *Biological psychiatry*, vol. 67, no. 7, pp. 672–678, 2010.

[12] J. D. Murray, A. Anticevic, M. Gancsos, M. Ichinose, P. R. Corlett, J. H. Krystal, and X.-J. Wang, "Linking microcircuit dysfunction to cognitive impairment: effects of disinhibition associated with schizophrenia in a cortical working memory model," *Cerebral cortex*, vol. 24, no. 4, pp. 859–872, 2014.

[13] S. Nobukawa, N. Wagatsuma, T. Ikeda, C. Hasegawa, M. Kikuchi, and T. Takahashi, "Effect of steady-state response versus excitatory/inhibitory balance on spiking synchronization in neural networks with log-normal synaptic weight distribution," *Cognitive Neurodynamics*, vol. 16, no. 4, pp. 871–885, 2022.

[14] N. Wagatsuma, S. Nobukawa, and T. Fukai, "A microcircuit model involving parvalbumin, somatostatin, and vasoactive intestinal polypeptide inhibitory interneurons for the modulation of neuronal oscillation during visual processing," *Cerebral Cortex*, 2022.

[15] S. Lefort, C. Tomm, J.-C. F. Sarria, and C. C. Petersen, "The excitatory neuronal network of the c2 barrel column in mouse primary somatosensory cortex," *Neuron*, vol. 61, no. 2, pp. 301–316, 2009.

[16] J.-n. Teramae, Y. Tsubo, and T. Fukai, "Optimal spike-based communication in excitable networks with strong-sparse and weak-dense links," *Scientific reports*, vol. 2, no. 1, pp. 1–6, 2012.

[17] V. S. Anishchenko, M. Safonova, and L. O. Chua, "Stochastic resonance in the nonautonomous chua's circuit," *Journal of Circuits, Systems, and Computers*, vol. 3, no. 02, pp. 553–578, 1993.

[18] R. Benzi, A. Sutera, and A. Vulpiani, "The mechanism of stochastic resonance," *Journal of Physics A: mathematical and general*, vol. 14, no. 11, p. L453, 1981.

[19] K. Wiesenfeld and F. Moss, "Stochastic resonance and the benefits of noise: from ice ages to crayfish and squids," *Nature*, vol. 373, no. 6509, pp. 33–36, 1995.

[20] M. Lukoševičius and H. Jaeger, "Reservoir computing approaches to recurrent neural network training," *Computer Science Review*, vol. 3, no. 3, pp. 127–149, 2009.

[21] M. Lukoševičius, "Echo state networks with trained feedbacks," 2007.

[22] G. Tanaka, T. Yamane, J. B. Héroux, R. Nakane, N. Kanazawa, S. Takeda, H. Numata, D. Nakano, and A. Hirose, "Recent advances in physical reservoir computing: A review," *Neural Networks*, vol. 115, pp. 100–123, 2019.

[23] Y. Kawai, J. Park, and M. Asada, "A small-world topology enhances the echo state property and signal propagation in reservoir computing," *Neural Networks*, vol. 112, pp. 15–23, 2019.

[24] F. Damicelli, C. C. Hilgetag, and A. Goulas, "Brain connectivity meets reservoir computing," *BioRxiv*, 2021.

[25] X. Li, W. Wang, F. Xue, and Y. Song, "Computational modeling of spiking neural network with learning rules from stdp and intrinsic plasticity," *Physica A: Statistical Mechanics and its Applications*, vol. 491, pp. 716–728, 2018.

[26] I. Matsumoto, S. Nobukawa, N. Wagatsuma, and T. Kurikawa, "Long-tailed distribution of excitatory postsynaptic potentials enhances learning performance of liquid state machine," *IEICE Proceedings Series*, vol. 71, no. B1L-E-01, 2022.

[27] S. Kang, K. Kitano, and T. Fukai, "Structure of spontaneous up and down transitions self-organizing in a cortical network model," *PLoS computational biology*, vol. 4, no. 3, p. e1000022, 2008.

[28] C. M. Lewis, A. Baldassarre, G. Committeri, G. L. Romani, and M. Corbetta, "Learning sculpts the spontaneous activity of the resting human brain," *Proceedings of the National Academy of Sciences*, vol. 106, no. 41, pp. 17 558–17 563, 2009.

[29] T. Sakaguchi and N. Wakamiya, "Consideration on liquid structure contributing to discrimination capability of liquid state machine," *Nonlinear Theory and Its Applications, IEICE*, vol. 11, no. 1, pp. 36–59, 2020.

[30] W. Maass, "Liquid state machines: motivation, theory, and applications," *Computability in context: computation and logic in the real world*, pp. 275–296, 2011.

[31] I. Matsumoto, S. Nobukawa, N. Wagatsuma, and T. Kurikawa, "Functionality of neural dynamics induced by long-tailed synaptic distribution in reservoir computing," *Nonlinear Theory and Its Applications, IEICE*, vol. 14, no. 2, pp. 342–355, 2023.

[32] J. Kujala, J. Jung, S. Bouvard, F. Lecaignard, A. Lothe, R. Bouet, C. Ciumas, P. Ryvlin, and K. Jerbi, "Gamma oscillations in v1 are correlated with gabaa receptor density: A multi-modal meg and flumazenil-pet study," *Scientific reports*, vol. 5, no. 1, p. 16347, 2015.

[33] R. Tatti, M. S. Haley, O. K. Swanson, T. Tselha, and A. Maffei, "Neurophysiology and regulation of the balance between excitation and inhibition in neocortical circuits," *Biological psychiatry*, vol. 81, no. 10, pp. 821–831, 2017.

[34] K. B. Quast, R. K. Reh, M. D. Caiati, N. Kopell, M. M. McCarthy, and T. K. Hensch, "Rapid synaptic and gamma rhythm signature of mouse critical period plasticity," *Proceedings of the National Academy of Sciences*, vol. 120, no. 2, p. e2123182120, 2023.

[35] S. Nobukawa, H. Nishimura, and T. Yamanishi, "Temporal-specific complexity of spiking patterns in spontaneous activity induced by a dual complex network structure," *Scientific reports*, vol. 9, no. 1, pp. 1–12, 2019.

[36] S. Nobukawa, N. Wagatsuma, and H. Nishimura, "Deterministic characteristics of spontaneous activity detected by multi-fractal analysis in a spiking neural network with long-tailed distributions of synaptic weights," *Cognitive Neurodynamics*, vol. 14, no. 6, pp. 829–836, 2020.

[37] H. Jaeger, "Short term memory in echo state networks," 2001.

[38] N. Brunel and X.-J. Wang, "Effects of neuromodulation in a cortical network model of object working memory dominated by recurrent inhibition," *Journal of computational neuroscience*, vol. 11, no. 1, pp. 63–85, 2001.

[39] X.-J. Wang and J. H. Krystal, "Computational psychiatry," *Neuron*, vol. 84, no. 3, pp. 638–654, 2014.

[40] D. A. Lewis, D. W. Volk, and T. Hashimoto, "Selective alterations in prefrontal cortical gaba neurotransmission in schizophrenia: a novel target for the treatment of working memory dysfunction," *Psychopharmacology*, vol. 174, pp. 143–150, 2004.

[41] N. Gogolla, J. J. LeBlanc, K. B. Quast, T. C. Südhof, M. Fagiolini, and T. K. Hensch, "Common circuit defect of excitatory-inhibitory balance in mouse models of autism," *Journal of neurodevelopmental disorders*, vol. 1, no. 2, pp. 172–181, 2009.

[42] G. A. Light, J. L. Hsu, M. H. Hsieh, K. Meyer-Gomes, J. Sprock, N. R. Swerdlow, and D. L. Braff, "Gamma band oscillations reveal neural network cortical coherence dysfunction in schizophrenia patients," *Biological psychiatry*, vol. 60, no. 11, pp. 1231–1240, 2006.